Geofluids (2007) 7, 415–426 doi: 10.1111/j.1468-8123.2007.00195.x

Analysis of the role of fluids in causing fractures in the Spraberry Trend, Midland Basin

B. J. MCPHERSON[1] AND D. F. BOUTT[2]

[1]*Energy & Geoscience Institute and Department of Civil and Environmental Engineering, University of Utah, Salt Lake City, UT, USA;* [2]*Department of Geosciences, University of Massachusetts – Amherst, Amherst, MA, USA*

ABSTRACT

The Spraberry Formation in west-central Texas is a highly fractured formation with both extension and shear fractures. At least two sets of natural fractures exist in two reservoir intervals. We have considered two possible origins for the fracturing: (i) high fluid pressure plus tectonic stress and (ii) tectonic stress at near-hydrostatic fluid pressure. Reconstruction of geologic, thermal and hydrodynamic histories suggests that high fluid pressures probably did not occur during the basin's history. To explore the second hypothesis, we developed and applied a calibrated, discrete-element model of Spraberry strata to investigate whether weak Laramide compressional forces could cause fractures in the absence of high fluid pressures. Simulation results suggest that a mild compressional episode of geologically short duration may indeed have induced conjugate shear fractures.

Key words: basin analysis, fractures, over pressures, strain, stress, thermal histories

Received 11 July 2007; accepted 12 July 2007

Corresponding author: B. J. McPherson, Energy and Geosciences Institute and Department of Civil and Environmental Engineering, University of Utah, Salt Lake City, UT 84112, USA.
Email: b.j.mcpherson@utah.edu. Tel: +1 801 581 5634. Fax: +1 801 585 3540.

Geofluids (2007) 7, 415–426

INTRODUCTION AND MOTIVATION FOR STUDY

The hydrodynamic regimes of deep sedimentary basins are usually affected by and often controlled by fractures (McCaig 1989; Forster & Evans 1991; Nordqvist *et al.* 1992; Bai *et al.* 1993; Caine *et al.* 1996). Fractures form in the presence of fluids with fluid pressures at or above hydrostatic (e.g., Hubbert & Rubey 1959; Secor 1965; Atkinson 1984; Pollard & Aydin 1988; Boone & Ingraffea 1990; Lorenz *et al.* 1991; Cheng *et al.* 1993; Renshaw & Harvey 1994). Secor (1965) used the concept of effective stress outlined by Hubbert & Rubey (1959) to show that tensile fractures form under compressive stress if pore fluid pressures are great enough. Boone & Ingraffea (1990) and Renshaw & Harvey (1994) focused on poroelasticity and crack-tip modeling using sophisticated, coupled, finite-element and finite-difference models. This study builds on these earlier works; here, we examine whether elevated fluid pressures contributed to fracturing of the Spraberry Formation in west-central Texas (Fig. 1).

The Spraberry Formation in the Midland Basin, Texas, is a highly fractured formation and has been deemed the 'largest uneconomic oil field in the world' (Guevara 1988). Fractures in the Spraberry have been attributed to many different mechanisms. Changes in sediment volume caused by compaction, regional tension and local uplift were cited by Warn & Sidwell (1953) and Guevara (1988). Another hypothesis is that the fractures are due to a weak force sustained over a long period of time (Schmitt 1954). Winfree (1995) and Lorenz *et al.* (2002) suggested that compressional forces exerted during the Laramide orogeny are the primary cause of fracturing, while Sterling (2000) suggested that high fluid pressures during the basin's history likely played an important role, consistent with results of previous studies of the coupling between fluid pressure and rock strain (e.g., Renshaw & Harvey 1994; McPherson & Garven 1999).

GEOLOGIC SETTING AND OBSERVED FRACTURES

The Midland Basin consists of shallow-marine shelf to shelf-margin carbonate and deep-basin deposits of

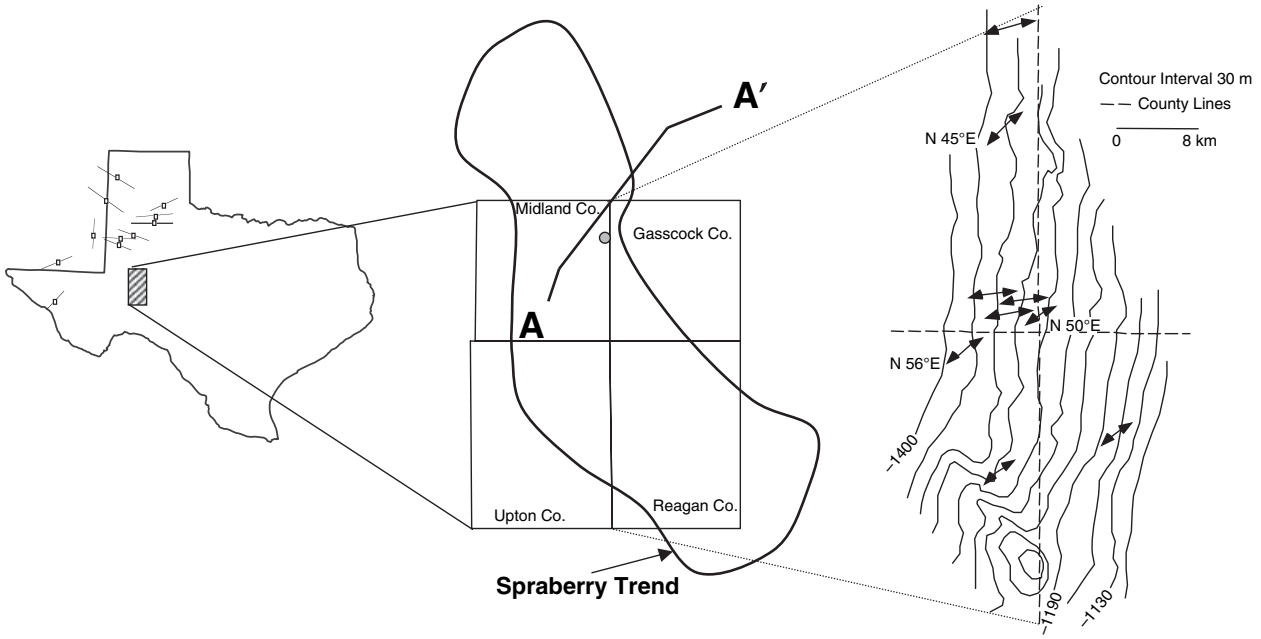

Fig. 1. Structure contour map of upper Spraberry Formation (right; from Barba 1989) illustrating the relatively simple structure of the area. Location of contour map area shown on map of Texas (left). Shown on the contour map are fracture orientations (determined by Barba 1989); shown on the map of Texas are major horizontal compressive stress orientations (from Zoback & Zoback 1989). Outline of Spraberry Trend and location of cross-section A-A′ shown in center schematic. The circle symbol located just south of the cross-section and near the Midland County line is the approximate location of the E.T. O'Daniel well.

Pennsylvanian and Permian age (Galley 1958; Handford 1981; Guevara 1988). Figure 1 includes a structure-contour map of the upper Spraberry Formation (adapted from Barba 1989) for a 64 km by 31 km area within the basin, illustrating that it is generally homoclinal, with a gentle westward dip of less than 1° extending into the deepest part of the basin. Table 1 lists the formations of interest in the basin, including dominant lithologies. The Spraberry consists of interbedded sandstone and shale and ranges in thickness from 200 m at the basin margins to 400 m at its depositional center (Stanley *et al.* 1951; Guevara 1988). In recent literature, the Spraberry is divided into sub-units, primarily to distinguish between areas of high and low oil production (Guevara 1988; Lorenz *et al.* 2002). In particular, the 10- to 15-feet-thick '1U' and '5U' sands of the Spraberry are designated are the most productive reservoir units in the trend (Lorenz *et al.* 2002).

Extensive natural fractures are observed in the Spraberry, despite its stable geologic setting with minimal folding and faulting (Lorenz *et al.* 2002). Analysis of horizontal core from the E. T. O'Daniel no. 28 well indicated a minimum of three sets of fractures in the upper Spraberry (Fig. 2). The three sets differ with respect to orientation, location, spacing, type and mineralization. The first set consists of extension fractures with a northeast strike (average 43°; Fig. 2). These fractures are limited to the 1U sand and silt reservoir facies, and have a low variability in strike (Lorenz *et al.* 2002). The second set consists of right-lateral shear fractures in sand and silt layers in the 5U that strike north–northeast (average 32°). The last fracture set strikes east–northeast (average 70°), and also includes extension fractures. This set is observed within the 5U-reservoir sand and silt unit, as well as within the black shales that overlie both the 1U and 5U reservoirs.

Hypothesis I: Elevated fluid pressures aided fracture formation

The observed structure and inferred geologic history of the Midland Basin suggests that it was not subject to major tectonic compressive stresses, but continually subsided from the time of Spraberry deposition until the Laramide orogeny. The focus of Laramide compressional thrusting events was hundreds of kilometers distant to the west–northwest. Folding of the local strata is relatively weak, and fractures do not show a strong correlation with local folding. These observations suggest a possible role of high fluid pressures: did overpressures reduce effective stresses sufficiently that minor compressional forces could induce the observed fractures?

Pervasive extension fractures also suggest that fluid pressure could have played a role in fracturing. Extension fractures form under different stress conditions than shear fractures, but both can be induced by elevated fluid

Table 1 Sedimentary strata of the Midland Basin, showing grouping of stratigraphic units for individual layers of the basin-evolution model (left-most column); the thickness of those units at the center of the basin; the beginning and ending time of deposition of those units; thermal conductivity values assigned to each unit; and the average sedimentation rate for the Spraberry Formation and all units younger than the Spraberry. Data summarized from Sterling (2000).

Layer number	Formation name	Lithology	Thickness(M)	Time		Thermal conductivity	Average sedimentation rate (m Myr^{-1})
				Start	End		
1	Fredericksburg	Limestone	24	106	72	2.5	0.1
1	Paluxy	Sandstone	24	140	106	3.5	0.1
	Unconformity			200	140		
2	Chinle	Sandstone shale	192	219.5	200	3	6
2	Santa Rosa	Shale	120	230	219.5	3.2	6
	Unconformity			250	230		
3	Dewey Lake	Sandstone	120	251.6	250	3.5	39
4	Rustler	Salt	60	253.3	251.6	4.5	49
		Anhydrite sandstone					
4	Salado	Salt	192	255	253.3	5	49
4	Tansill	Anhydrite sandstone	72	255.8	255	4.5	49
4	Yates	Anhydrite sandstone	120	257	255.8	4.5	49
5	Seven Rivers	Salt	108	258.1	257	5	146
		Anhydrite sandstone					
6	Queen	Salt	192	260	258.1	4.8	66
		Anhydrite sandstone					
7	Grayburg	Dolomite Limestone	120	261.2	260	4	104
8	San Andres	Sandstone limestone	360	264.8	261.2	3	133
9	Word/Leonardian	Sandstone shale	528	270	264.8	2.8	42
10	Spraberry	Sandstone shale	288	273	270	3.1	22
11	Unnamed Shale		144	274	273	2.5	
11	Dean	Sandstone	48	275	274	3.5	
12	Wolfcamp	Limestone shale	432	290	275	2.5	
	Unconformity			308	290		
	Strawn	Limestone	48	312	308	2.5	
	Bend	Limestone shale	192	325	312	2.5	
	Unconformity			330	325		
	Barnett	Shale	24	335	330	2.5	
	Unconformity			345	335		
	Mississipian	Limestone	24	365	345	2.5	
	Unconformity			380	365		
	Woodford	Shale	24	387	380	2.5	
	Unconformity			390	387		
	Devonian	Limestone	144	405	390	2.5	
	Silurian	Shale	48	417	405	2.5	
	Fusselman	Dolomite	24	420	417	4	
	Unconformity			425	420		
	Montoya	Limestone	24	455	425	2.5	
	Simpson	Limestone	24	485	455	2.5	
	Ellenburger	Dolomite	216	500	485	4	

pressure. Extension fractures lie in the σ_1 and σ_2 plane, indicating that σ_1 was between vertical and horizontal and trended northeast to east–northeast at the time of failure. The fact that we do not know whether the maximum compressive stress that caused the extension fractures was vertical or horizontal complicates the task of determining when they formed. Two sources of stress that could have lead to post-Laramide extensional fractures are loading by overlying sediment and horizontal compressive stresses produced by subsidence. Given the likelihood that both of these stresses were relatively weak, high fluid pressures could have been a critical factor. Luo (1992), Lee & Williams (2000) and Tuncay *et al.* (2000) all document overpressures in the Delaware Basin immediately to the west. Tuncay *et al.* (2000) evaluated the possible genetic relationship between observed high fluid pressures and fractures in the Delaware Basin.

Our primary objective was to determine the likelihood of overpressures and to elucidate whether such pressures are necessary for the genesis of observed Spraberry fractures in the Midland Basin. We tested two primary mechanisms for generating high fluid pressures: (i) sedimentary

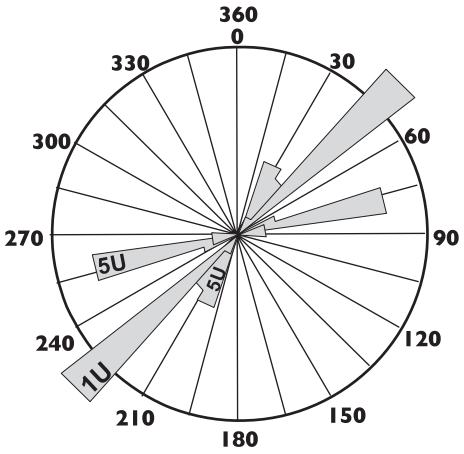

Fig. 2. Rose diagram of observed fracture sets in the Spraberry Formation.

compaction, such as observed in the Gulf Coast (Bethke 1986), and (ii) oil generation, as observed in the Uinta Basin of Utah (McPherson & Bredehoeft 2001). Lee & Williams (2000) suggested that these two mechanisms are responsible for overpressures in the Delaware Basin, although maintenance of overpressures from Permian (initiation of overpressure) to present day would require an extremely low-permeability ($<10^{-20}$ m^2) top seal.

Hypothesis II: Regional compression without elevated fluid pressures

Observed fractures in the Spraberry Formation (Fig. 2) provide a number of clues about the forces and orientations of stresses that caused them. The geometry of observed shear fracture sets suggests that, at the time of failure, σ_1 was horizontal and trended northeast. Two sets of surface lineaments and fractures striking northeast and northwest were observed and described by Stanley *et al.* (1951) and Guevara (1988) and were linked genetically to Spraberry shear fractures by Stanley *et al.* (1951). This suggests that Spraberry fractures formed since the deposition of surface sediments in the early Cretaceous, consistent with timing of the Laramide orogeny, ~80–55 Ma. The northeastern orientation of σ_1 is consistent with the direction of weak regional compressive forcing imparted by the Laramide orogeny. Recent sonic-velocity-anisotropy orientation measurements of Spraberry core suggest that present-day stresses are also oriented in the northeastern direction (Lorenz *et al.* 2002). Additionally, Winfree (1995) suggested that subsequent Laramide extension has helped maintain or keep fractures open. In summary, this evidence suggests that fractures in the Spraberry are at least related to the stress state deemed to be present during the Laramide compression event, whether caused exclusively by compressional forces and maintained by extension, or by a combination of these forces with elevated fluid pressures, as discussed below.

HYPOTHESIS TESTING AND RESULTS

Hypothesis I: Elevated fluid pressures aided fracture formation

In contrast to the neighboring Delaware Basin, overpressures are relatively scarce in the present-day Midland Basin. We tested the hypothesis of overpressure-induced fractures by examining whether overpressures were likely to have occurred there in the geologic past. We selected a north–northeast cross-section (Jones 1953) for hydrodynamic analysis (location of profile shown on Fig. 1; cross-section model grid and associated stratigraphic definition depicted in Fig. 3). We selected this orientation on the basis of current horizontal-compressive-stress directions (Zoback & Zoback 1989) and the general north–northeast direction of many observed fractures. This two-dimensional representation of the basin is sufficient for testing the hypotheses in question and permits simulation of representative burial histories, thermal histories, petroleum generation and patterns of multiphase flow.

Numerical model of basin evolution

We simulated the geologic, thermal, hydrodynamic and petroleum-generation histories of the Midland Basin cross-section using the basin-evolution model developed and described by McPherson & Bredehoeft (2001). The TOUGH2-DYME model (McPherson & Bredehoeft 2001) simulates physical basin evolution and includes coupled heat and multiphase (oil/gas/water) fluid flow, and is based on the integrated-finite-difference method employed

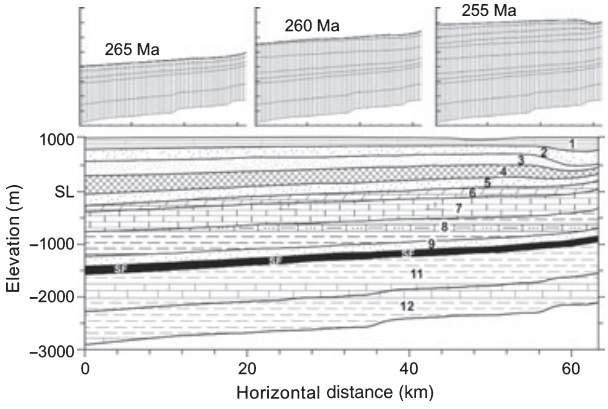

Fig. 3. Top three panels show the model grid of the structural cross-section at selected times. The bottom panel shows the stratigraphy for the structural cross-section; patterns indicate different rock types, with details of the rock types provided in Table 1. 'SF' indicates Spraberry Formation. The top three panels employ the same axis scales as the bottom panel. Cross-section adapted from Jones (1953).

in TOUGH2 (Pruess 1991). We assembled a two-dimensional integrated-finite-difference grid of 65 columns by 14 rows, each cell 3200 feet wide and having a thickness equal to the stratigraphic thickness represented. The model builds and evolves the grid through geologic time. Sedimentation rates were estimated by conventional backstripping and are tabulated in Table 1. Figure 3 illustrates the basin model grid (cross-section A-A′) at three selected stages of the basin's history.

Rock and fluid properties required to parameterize the basin-evolution model include porosity, permeability, thermal conductivity, petroleum-generation parameters, and oil density and viscosity. For simulating forward-in-time evolution of the basin, rock properties must be assigned some initial condition or value at the onset of deposition, and follow a specified trend as a function of location (e.g., depth) or physical condition (e.g., fluid pressure or effective stress). For forward simulation of porosity in all units, we used a simple consolidation law (Sclater and Christie, 1980) with porosity a function of stress:

$$\phi = \phi_0 \exp\left[-\left\{\frac{c}{(\bar{\rho_b} - \rho_w)g}\right\}\sigma\right], \quad (1)$$

where ϕ is porosity, ϕ_0 is estimated initial (surface) porosity, c is a coefficient associated with rock type, ρ_b is bulk sediment density, ρ_w is water density, g is acceleration of gravity, and σ is total stress; all of these variables are tracked in the simulator. In the absence of basin-specific parameter values for Eqn (1), we used estimated values based on the dominant lithology for each unit (Table 2).

For forward simulation of permeability in all units except the Spraberry, we implemented a Kozeny-Carman formula

Table 2 Compaction parameters assigned in the basin model, based on experimental work on dolomite/anhydrite cores and Kendall (1969), Schmoker & Halley (1982), Scholle (1980), and Sclater and Christie (1980). Specific surface area (S_o) values from Burrus *et al.* (1992) and Gonçalvès *et al.* (2004).

Lithology	Surface porosity φ_o	c (km^{-1})	S_o (m^{-1})
Sandstone	0.49	0.27	2.5×10^4
Shaley sandstone	0.56	0.39	2.1×10^5
Shale	0.63	0.39	3.1×10^5
Limestone	0.5	0.52	1×10^5
Dolomite/anhydrite	0.3	0.22	1.1×10^5

(adapted from Burrus *et al.* 1992; and Gonçalvès *et al.* 2004):

$$k = \frac{0.2(1-\phi)^3}{S_0^2\phi^2} \quad (2)$$

where k is intrinsic permeability, ϕ is porosity, and S_0 is specific surface area (Table 2). For the Spraberry unit we assigned permeability as a function of pore pressure calculated by the model. We calibrated the model using measured values of pressure-sensitive permeability of unfractured Spraberry samples (Sterling 2000). The measured permeability trend as a function of confining pressure and pore pressure is illustrated in Fig. 4. This trend was evaluated by measuring permeability for 12 core samples taken from the Spraberry. Unfortunately, permeability of silty shale and shale samples were too low to perform tests within a reasonable amount of time, so the trend shown in Fig. 4 is biased toward higher permeability horizons of the Spraberry. These permeability tests were performed concurrently with some of the triaxial shear tests, and used the same test

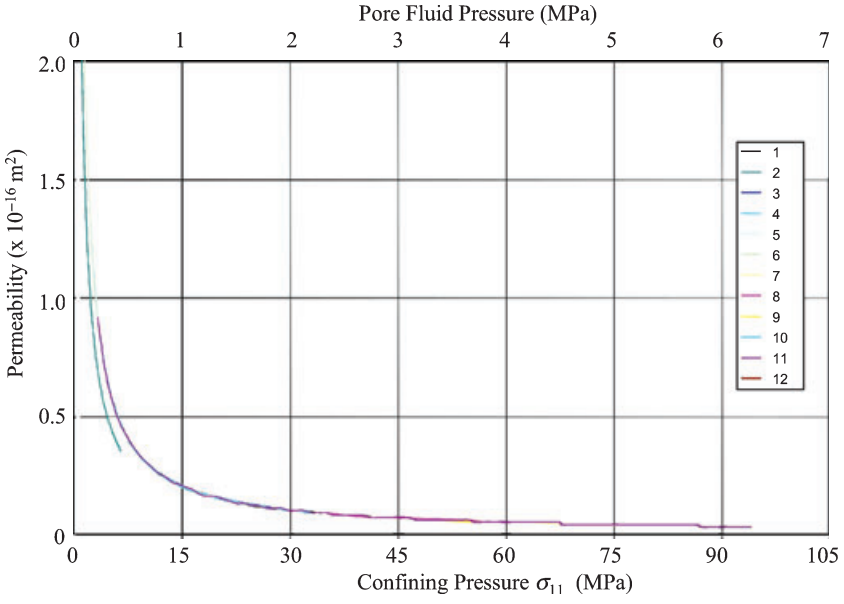

Fig. 4. Permeability as a function of pore pressure, based on measurements made during triaxial compression tests on 12 Spraberry Formation core samples. Testing methods and results described by Sterling (2000).

configuration with the addition of Isopar H mineral oil pumped into the bottom of the samples at a rate of 4 ml h^{-1}. The pore pressure at the point of injection was measured using pressure transducer, while axial and lateral displacement was measured using linear variable displacement transducers because strain gauges had a tendency to separate slightly from the sample when internal fluid pressure was applied. Using the measured pore pressure and fluid injection rate, it was possible to calculate the permeability of each sample using Darcy's law. During these tests, vertical load was applied for a period of time, and then stopped to permit the sample pressure to equilibrate, and then increases in load were resumed again. As illustrated by Fig. 4, permeability values dropped exponentially when increasing amounts of σ_{11} were applied, despite a contemporaneous increase in fluid pore pressure, most likely due to net compaction of pore space.

We assumed the Spraberry Formation to be oil source rock as well as reservoir strata, dominated by Type II kerogen because of its marine origin. A first order Arrhenius equation for oil generation with kinetic parameters appropriate to generic Type II kerogen was applied (Sweeney 1990), and details of its implementation in the basin evolution model are provided by McPherson & Bredehoeft (2001). We assigned a reported maximum value of 3.6% total organic carbon (TOC) to Spraberry strata (Dutton 1980) to maximize the effect of oil generation on fluid pressures. Oil density as a function of temperature and pressure was assigned with a formulation outlined by Eremenko (1991), while viscosity of oil (as a function of temperature and pressure) was assigned based on correlations of Beal (1946). We applied relative-permeability and capillary-pressure formulations described by Parker *et al.* (1987). Thermal boundary conditions were consistent with conditions described by Negraru *et al.* (2004), including constant heat flow into the base of the basin at 46 mW m^{-2}, the average heat flow for the area of the Midland Basin. The sides of the basin model were assigned no-flow with respect to heat conduction. A constant head equal to a mean water elevation of 100 feet (30 m) was assigned at the surface of the domain consistent with local depth to water-table in the Midland area reported by Jackson *et al.* (2004). Basement rocks below the simulated stratigraphic section provide a low-permeability barrier that justifies a no-flow boundary along the bottom of the model domain. No-fluid-flow boundaries were assigned to the northeastern side (A′) of the model domain on the basis of topographic symmetry. A specified fluid flow boundary was assigned along the northeastern side boundary, based on fluid flux rates, ranging from 19 m $year^{-1}$ in upper units to 0.06 m $year^{-1}$ in deeper units, inferred by simple Darcy's law calculations using local head gradients reported by Jackson *et al.* (2004).

Geologic history

The geologic history of the basin is relatively simple. Figure 5A shows the complete burial history for the E.T. O'Daniel no. 28 well, located at the approximate center of the north–northeast cross-section. After backstripping and using the depositional parameters summarized in Table 1, we simulated the basin's history and resulting temperature, oil generation, and fluid-pressure histories (Fig. 5B–D, respectively).

The basin began forming between 310 and 265 Ma (Hill 1995) and all basin simulations commence at 273 Ma (Fig. 5) when the Spraberry began to be deposited. From

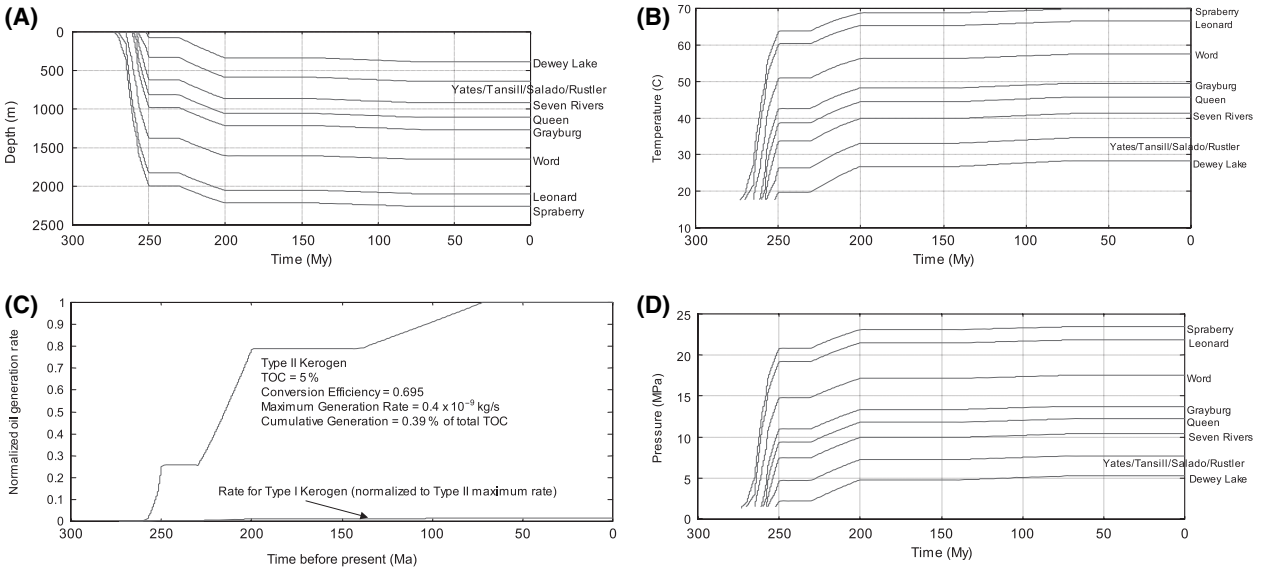

Fig. 5. Model simulation results for Midland Basin strata at E.T. O'Daniel well, including (A) depth histories, (B) temperature histories, (C) oil-generation-rate histories, and (D) fluid-pressure histories.

250 to 230 Ma the basin subsided and was covered by a shallow sea that eventually receded, producing evaporite deposits (Hill 1995). An unconformity records the erosion of the uppermost Permian sediments, including any additional strata deposited around 250 Ma (Boggs 1995). In our basin model (Fig. 5A), deltaic and lacustrine sediments were deposited from 230 to 200 Ma. However, another unconformity in the stratigraphic column marks removal of all sediments deposited between 230 and 140 Ma. The youngest formations that remain today are shallow marine deposits ranging in age from 140 to 72 Ma (Fig. 5A).

Thermal history

The simulated temperature history for strata at the center of the basin cross-section is plotted in Fig. 5B. Temperatures track depth, with conduction the dominant mechanism. Advection of heat by fluid flow was negligible in all simulations.

Oil-generation history

Oil generated from kerogen in the Spraberry begins forming around 3 Myr into the basin history simulation, or ~270 Ma (Fig. 5C), with a peak in generation occurring about 74 Ma and continuing until present day. However, generation rates were not sufficiently high to affect fluid pressures. The maximum generation rate is relatively low, 0.4×10^{-9} kg sec^{-1}, primarily because temperature in the Spraberry remains very low in the oil window ≤70°C. Significantly higher generation rates can increase fluid pressures inasmuch as the conversion of solid kerogen to oil of lower density results in an increase in fluid volume (Bredehoeft *et al.* 1994; Burrus 1998; Lee & Williams 2000; McPherson & Bredehoeft 2001). Figure 5C illustrates the oil-generation-rate history for the Spraberry corresponding to the base-case basin-evolution model. The model also produced oil-migration histories, and these simulated migration histories and resulting distributions of oil are at least qualitatively consistent with present-day production maps, but we do not present those here for the sake of brevity and because this aspect is beyond the hypothesis-testing scope of this study.

Fluid pressure histories

The main goal of the basin modeling was to determine whether very high fluid pressures were the cause of observed fractures. Extremely high overpressures may cause extension fractures by exceeding the least principal stress, whereas moderately high overpressures may contribute to shear fracturing by reducing effective stress. Our model results suggest that no significant overpressuring occurred. Pressures in the Spraberry correspond to the top-most line on Fig. 5D, and track close to hydrostatic conditions throughout the basin history, reaching a maximum of approximately 23 MPa at a depth of ~2300 m. No overpressures occur during any part of the simulated basin history, at least not for the model assembled and parameterized based on what we deem to be the most reasonable conceptual model.

We performed a sensitivity study to determine what conditions might create significant overpressures. Results suggested that sedimentation rates would need to be at least 10 times greater than backstripped rates to induce significant overpressures. Sensitivity analysis of permeability was similarly limiting: for significant overpressures to form, the Spraberry, San Andres, Word and Grayburg units all needed to have permeabilities of 10^{-18} m^2 or less, consistent with our previous studies of overpressuring (e.g., McPherson & Bredehoeft 2001).

Testing Hypothesis II: Regional compression without elevated fluid pressures

We turn our attention to whether or not inferred low strain rates associated with the Laramide orogeny could induce significant fracturing, unaided by high fluid pressures. This issue is addressed using a two-dimensional discrete-element-method (DEM) modeling approach.

DEM model of Laramide compression

The DEM entails simulating the mechanical behavior of rock by idealizing the system as a collection of structural units (springs, beams, etc.) or separate particles bonded together at their contact points, utilizing the breakage of individual structural units or bonds to represent damage (Cundall & Strack 1979; Cundall 1986). Each particle has unique properties and represents a collection of mechanical units. The particles do not represent grains, but are meant to discretize space much like cells or elements in continuum models. This method has an inherent ability to represent damage or fractures in a direct fashion as well as producing realistic nonlinear behavior using simple contact laws governed by Newtonian mechanics (Saltzer & Pollard 1992; Hazzard *et al.* 2000). Details of model input parameters and algorithms are provided by Boutt & McPherson (2002) and Potyondy *et al.* (1996).

Our DEM model was calibrated to the measured mechanical properties of the Spraberry Formation (Sterling 2000). The measured mechanical yield strengths from Sterling (2000) and Lorenz *et al.* (2002) indicated that portions of the Spraberry are weak relative to other units: the average yield strength of the lower 5U sandstone is ~150 MPa (Sterling 2000; Lorenz *et al.* 2002) and the average yield strength of the upper 1U sandstone is ~263 MPa. Lorenz *et al.* (2002) show that these differences in strength (which we assume to be representative of rock strength during fracturing) result from subtle differences in quartz and clay content. Details of the calibration process are described by Boutt & McPherson

(2002). Rocks from each individual sub-unit of the Spraberry Formation were calibrated separately and the parameters recorded.

The DEM assemblies were built by generating particles with a uniform normal distribution to completely fill the domain of interest, then compacted until a low ($\sim$ 0.1 MPa) isotropic stress was achieved. The final step was assignment of parameters to the Spraberry model units. Boundary conditions assigned to the top and bottom of the model were constant stress (representing the minimum stress direction). This implies that the assembly can strain from the top and the bottom, but the overall stress will remain constant. This is justified because the assembly was loaded to emulate burial conditions imposed on the unit during the Laramide orogeny. The boundary conditions on the sides of the model were assigned as constant strain rate. Few strain or shortening rates for the Midland Basin exist, and therefore we used a strain rate typical of mildly compressive regions (Twiss & Moores 1992): a rate of 3×10^{-17} sec^{-1} was applied for 5.4 Ma, inducing a cumulative strain of 0.0051 or 0.51% in the direction of compression. Lorenz *et al.* (2002) reported a strain of 0.1% for extension fractures parallel to the assumed maximum stress direction during the Laramide. Given that this strain is normal to the direction of compression and the small Poisson's ratio reported for these rocks (0.03–0.11), our value of strain rate appears appropriate. Our value is also consistent with the lack of structures found within the Midland Basin (Winfree 1995).

Our DEM modeling results are limited by the two-dimensionality of the model. The fractures in the Spraberry Formation are three-dimensional structures. In this initial idealization, we chose to model 2-D horizontal sections parallel to the assumed shortening direction. We are not able to resolve the exact orientation of fractures observed in the Spraberry Formation. Instead, we are attempting to determine whether, for a given set of material properties, the assumed strain rates were large enough to cause deformation in the Spraberry Formation.

Plots of results are generated by first gridding the cumulative displacements for all particles in the DEM model for a timestep and then taking the spatial gradients of the resultant vectors [see Boutt & McPherson (2002) for an example]. This technique highlights differential movements in the assembly. A fracture or fault marks a discontinuity in an otherwise coherent medium and thus will show a strong gradient of overall movement (cumulative displacement) with respect to a fixed coordinate system. Figure 6 depicts results and boundary conditions for a homogeneous one-layer model of the 5U section of the Spraberry Formation (see Table 3 for mechanical properties). The deformation field is very heterogeneous, highlighted by distinct regions of high-magnitude displacement gradients (brighter regions). Large displacement gradients exist throughout the model and are coincident with bond breakages (black lines) between the individual discrete elements.

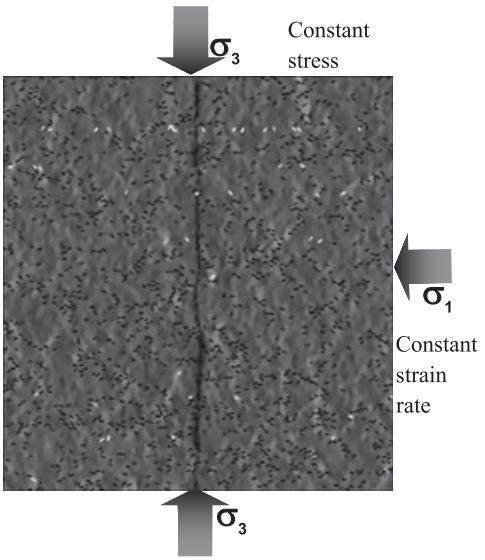

Fig. 6. Results of the 5U simulation showing boundary conditions. Spraberry Formation strata consist of thin reservoir sands surrounded by thicker, fine-grained silts and shales. Resultant displacement-gradient contours of the 5U model show significant deformation. It is possible that the properties of the surrounding units may influence how individual units behave mechanically.

Table 3 Elastic and inelastic data used in seven- and three-layer models.

Property	1U-3	5U-6	3-Layer model
Unconfined E (GPa)	42.1	20.8	20
Unconfined Poisson's ratio	0.088	0.112	0.03
Unconfined failure strength (MPa)	250.3	159.2	N/A
Bulk modulus (GPa)	Not calculated	Not calculated	12.2

We interpret these patterns to represent areas of strain localization where adjacent regions are undergoing differential movement. These areas represent discontinuities, in this case shear fractures, consistent with the interpretations of Lorenz *et al.* (2002). Even for the relatively small strain rates applied, distinct deformation zones form in the model. The relatively weak compression rates associated with the Laramide orogeny appear sufficient to induce deformation, without the need for excessive fluid pressures to reduce effective stress.

Analysis of stress amplifications via contrasts in rock mechanical properties

We suspect that mechanical interactions (both inelastic and elastic) or stress amplifications (see Eshelby 1957; Lorenz *et al.* 1991) among the units of the Spraberry Formation may cause variability in induced fractures. The elastic and

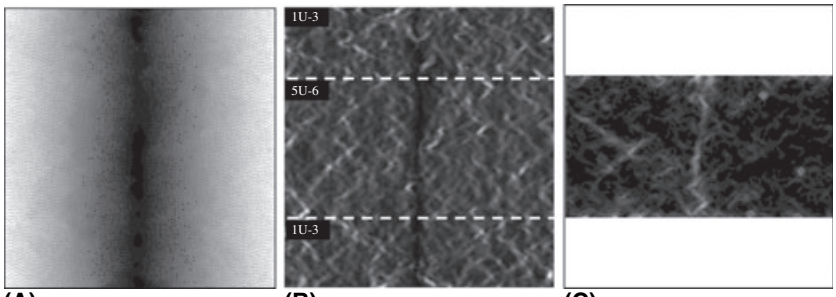

Fig. 7. DEM simulation results: (A) Cumulative particle displacements and associated displacement vectors; (B) spatial displacement gradients; and (C) residual displacement gradients of middle layer.

inelastic behavior of any given rock unit may be influenced by the surrounding rock units. Thus the effective elastic and inelastic properties of a suite of units may be different from the properties of the individual units.

To evaluate this possibility, scaled DEM models of the Spraberry Formation stratigraphy were assembled using calibrated parameters. We assembled three-layer models in the vertical direction (Fig. 7), rather than a homogeneous model in the horizontal direction (Fig. 6), attempting to capture the physics of mechanical interactions between layers. The top and bottom boundary conditions were set to the overburden load as determined via the basin evolution model. We examined several different scenarios invoking material properties of the Spraberry Formation (Table 3). The model discussed here is a 5U reservoir sandstone sandwiched between two equally thick 1U shales. Heterogeneous units (mechanical stratigraphy) influence each other in terms of their abilities to transfer and deflect stresses.

Simulation results are depicted in Fig. 7. This model has two equally thick outer layers (50% of total thickness) with the properties of the Spraberry Formation unit 1U-3 and one middle layer of the 5U-6, unit which also makes up 50% of the thickness. The geometry is illustrated in Fig. 7B by the dashed lines. The 1U-3 unit is much stronger and stiffer than the 5U-6 unit. The strength of the bonds between layers was assigned as the average of the 1U-3 and 5U-6 layers. Results suggest that this heterogeneity has a strong influence on the behavior of the systems. Figure 7A depicts a gridded, filled contour plot of cumulative spatial displacement. The overall direction of displacement is horizontal and toward the center, indicative of compression. Spatial displacement gradients of this field (Fig. 7B) show heterogeneous deformation.

To isolate or highlight contrasts in behavior between the two units, we subtracted the 5U-6 displacement gradient results shown in Fig. 7B from those for a 1-layer (i.e., homogeneous) model with the properties of the 5U-6 unit (Fig. 7C). The organization of the displacement gradients of the 5U-6 layer suggests that this layer is undergoing strain localization differently than is observed for the homogeneous case.

Lastly we examined the effect of relative proportions of 1U and 5U on the overall failure behavior of an ensemble. Simulations with 0%, 25%, 50%, 75%, and 100% 1U units were generated. We loaded the layered system until bulk failure, as determined by a loss in strength of the assembly, and the time of failure was noted.

Figure 8 shows stress parallel to loading versus time to failure for assemblies composed of the different percentages of 1U and 5U units. The two end-members, 0% and 100% 1U, show very different magnitudes and the timing of peak stress. The 100% 1U simulation reaches peak stress first and attains the highest stress whereas the 0% 1U simulation shows the lowest peak stress reached after the longest amount of time. The more brittle 100% 1U simulation shows a pronounced failure peak whereas the 0% 1U simulation shows a more rounded and smoothed peak.

There is a nonlinear transition from 0% to 100% 1U behavior. The 25% 1U is much stronger than the 0% 1U and also fails much sooner. Its strain curve is more like that of the 100% 1U simulation than the 0% 1U simulation. Even small percentages of the stronger and more brittle 1U units influence the mechanical behavior of the package as a whole.

SUMMARY AND CONCLUSIONS

We evaluated two competing hypotheses for the origin of fractures in the Spraberry Formation of the Midland Basin, Texas that invoke (i) significant subsurface fluid overpressures or (ii) tectonic compression with near-hydrostatic fluid pressures. Simulated geologic, thermal and hydrodynamic histories suggest that high fluid pressures probably did not occur during the basin's history, and thus did not play a significant role in fracturing. To test the second hypothesis, we developed and applied a calibrated, discrete-element model of Spraberry strata. Simulation results suggest that a mild compressional episode may have induced conjugate shear fractures without excessive fluid pressures. We find that

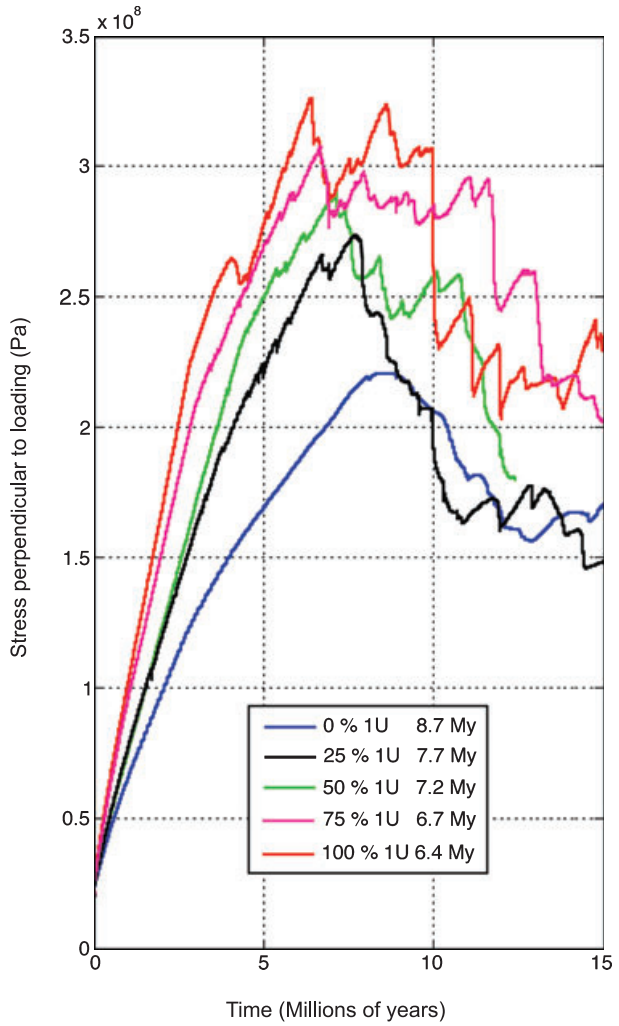

Fig. 8. Stress parallel to loading as a function of simulation time for assemblies composed of the stated percentages of 1U and 5U units. The varying percentages affect both the strength of the unit and the timing of failure.

(1) significant overpressures likely did not form during the Midland Basin's history, in contrast to its sister basin, the Delaware Basin;
(2) observed extension fractures are not hydraulic in nature;
(3) a mild compressional episode of geologically short duration may have induced Spraberry fractures, including observed types and orientations, without excessive fluid pressure; and
(4) mechanical interaction between the Spraberry Formation subunits can account for some observed differences in fracture patterns.

ACKNOWLEDGEMENTS

The authors would like to thank Jenny Sterling who completed many of the laboratory measurements used in this analysis for her M.S. thesis project in 2000. The University of Utah provided computational facilities for the simulations detailed in this study, in association with a sabbatical visit by the senior author. Partial funding for the rock/site characterization portion of the study was provided by the U.S. Department of Energy, project DE-PS26-O3NT41983.

REFERENCES

Atkinson BK (1984) Subcritical crack growth in geological materials. *Journal of Geophysical Research*, **89**, 4077–114.
Bai MD, Elsworth D, Roegiers J (1993) Multiporosity/multipermeability approach to the simulation of naturally fractured reservoirs. *Water Resources Research*, **29**, 1621–33.
Barba RE (1989) Optimizing hydraulic-fracture length in the Spraberry Trend. *SPE Formation Evaluation*, **4**, 475–82.
Beal C (1946) The viscosity of air, water, natural gas, crude oil and its associated gases at oil-field temperatures and pressures. *Transactions AIME*, **165**, 94–115.
Bethke CM (1986) Inverse hydrologic analysis of the distribution and origin of gulf coast-type geopressured zones. *Journal of Geophysical Research*, **91**, 6535–45.
Boggs S Jr (1995) *Principles of Sedimentology and Stratigraphy*, 2nd edn, Prentice Hall, Englewood Cliffs, NJ.
Boone TJ, Ingraffea AR (1990) A numerical procedure for simulation of hydraulically-driven fracture propagation in poroelastic media. *International Journal for Numerical and Analytical Methods in Geomechanics*, **14**, 27–47.
Boutt DF, McPherson BJOL (2002) Simulation of sedimentary rock deformation: lab-scale model calibration and parameterization. *Geophysical Research Letters*, **29**, 10.1029/2001GL013987.
Bredehoeft JD, Wesley JB, Fouch TD (1994) Simulations of the origin of fluid pressure, fracture generation, and the movement of fluids in the Uinta Basin, Utah. *American Association of Petroleum Geologists Bulletin*, **78**, 1729–47.
Burrus J (1998) Overpressure models for clastic rocks, their relation to hydrocarbon expulsion: a critical reevaluation, in abnormal pressures in hydrocarbon environments. *American Association of Petroleum Geologists Memoir*, **70**, 35–63.
Burrus J, Kuhfuss A, Doligez B, Ungerer P (1992) Are numerical models useful in reconstructing the migration of hydrocarbons? A discussion based on the Northern Viking Graben. In: *Petroleum Migration* (eds England WA, Fleet AJ). *Geological Society of London Special Publication*, **59**, 89–109.
Caine JS, Evans JP, Forster CB (1996) Fault zone architecture and permeability structure. *Geology*, **24**, 1025–8.
Cheng AHD, Abousleiman Y, Roegiers JC (1993) Review of some poroelastic effects in rock mechanics. *International Journal of Rock Mechanics and Mining Sciences and Geomechanics Abstracts*, **30**, 1119–26.
Cundall PA (1986) Distinct element models of rock and soil structure. In: *Analytical and Computational Methods in Engineering Rock Mechanics* (ed. Brown ET), pp. 129–63. Allen & Unwin, London.
Cundall PA, Strack ODL (1979) A discrete element model for granular assemblies. *Geotechnique*, **29**, 47–65.
Dutton SP (1980) *Petroleum Source Rock Potential and Thermal Maturity, Palo Duro Basin, Texas; Bureau of Economic Geology Circular 80-10*, The University of Texas at Austin, Austin, TX, 48 pp.
Eremenko NA (1991) *Petroleum Geology Handbook*. OSI Publications, Los Angeles, 600 pp.

Eshelby J (1957) The determination of the elastic field of an elliptical inclusion, and related problems. *Proceedings of the Royal Society A*, **241**, 376–396.

Forster CB, Evans JP (1991) Hydrogeology of thrust faults and crystalline thrust sheets; results of combined field and modeling studies. *Geophysical Research Letters*, **18**, 979–82.

Galley JE (1958) Oil and geology in the Permian basin of Texas and New Mexico. In: *Habitat of Oil* (ed. Weeks LG), pp. 395–446. American Association of Petroleum Geologists, Tulsa, OK.

Gonçalvès J, Violette S, Guillocheau F, Robin C, Pagel M, Bruel D, de Marsily G, Ledoux E (2004) Contribution of a three-dimensional regional scale basin model to the study of the past fluid flow evolution and the present hydrology of the Paris Basin, France. *Basin Research*, **16**, 569–86.

Guevara EH (1988) *Geological Characterization of Permian Submarine Fan Reservoirs of the Driver Waterflood Unit Spraberry Trend, Midland Basin, Texas; Report of Investigations No. 172.* Bureau of Economic Geology, Austin, TX.

Handford CR (1981) Sedimentology and genetic stratigraphy of Dean and Spraberry Formations (Permian), Midland Basin, West Texas. *American Association of Petroleum Geologists Bulletin*, **65**, 1602–16.

Hazzard JF, Young PF, Maxwell SC (2000) Micromechanical modeling of cracking and failure in brittle rocks. *Journal of Geophysical Research*, **105**, 16683–97.

Hill CA (1995) *Geology of the Delaware Basin Guadalupe, Apache and Glass Mountains, New Mexico and West Texas; Permian Basin Section*. SEPM Publication 96-39, Tulsa, OK.

Hubbert MK, Rubey WW (1959) Role of fluid pressure in mechanics of overthrust faulting. *Geological Society of America Bulletin*, **70**, 115–66.

Jackson WA, Rainwater K, Anderson T, Lehman T, Tock R, Rajagopalan S, Ridley M (2004) *Distribution and Potential Sources of Perchlorate in the High Plains Region of Texas: A Final Report to the Texas Commission on Environmental Quality*, Texas Tech University, Lubbock, TX.

Jones TS (1953) *Stratigraphy of the Permian Basin of West Texas.* West Texas Geological Society, Midland, TX, 63 pp.

Kendall CG (1969) An environmental re-interpretation of the Permian evaporite-carbonate shelf sediments of the Guadalupe Mountains. *Geological Society of America Bulletin*, **80**, 2503–26.

Lee M, Williams DD (2000) Paleohydrology of the Delaware Basin, western Texas; overpressure development, hydrocarbon migration, and ore genesis. *American Association of Petroleum Geologists Bulletin*, **84**, 961–74.

Lorenz JC, Teufel LW, Warpinski NR (1991) Regional fractures: I. A mechanism for the formation of regional fractures at depth in flat-lying reservoirs. *American Association of Petroleum Geologists Bulletin*, **75**, 1714–37.

Lorenz JC, Sterling JL, Schechter DS, Whigham CL, Jensen JL (2002) Natural fractures in the Spraberry Formation, Midland Basin, TX: the effects of mechanical stratigraphy on fracture variability and reservoir behavior. *American Association of Petroleum Geologists Bulletin*, **86**, 505–24.

Luo M (1992) *Generation and Development of the Overpressure System in the Eastern Delaware Basin, West Texas and Southern New Mexico.* PhD Dissertation, University of Texas at El Paso, El Paso, 206 pp.

McCaig AM (1989) Geology; fluid flow through fault zones. *Nature*, **340**, 600.

McPherson BJOL, Bredehoeft JD (2001) Overpressures in the Uinta basin, Utah: analysis using a three-dimensional basin evolution model. *Water Resources Research*, **37**, 857–72.

McPherson BJOL, Garven G (1999) Hydrodynamics and overpressure mechanisms in the Sacramento Basin, California. *American Journal of Science*, **299**, 429–66.

Negraru PT, Blackwell DD, Erkan K (2004) Heat flow in Texas. *American Association of Petroleum Geologists Annual Meeting Expanded Abstracts*, **13**, 104.

Nordqvist AW, Tsang YW, Tsang CF, Dverstorp B, Andersson J (1992) A variable aperture fracture network model for flow and transport in fractured rocks. *Water Resources Research*, **28**, 1703–13.

Parker JC, Lenhard RJ, Kuppusamy T (1987) A parametric model for constitutive properties governing multiphase flow in porous media. *Water Resources Research*, **23**, 618–24.

Pollard DD, Aydin A (1988) Progress in understanding jointing over the past century. *Geological Society of America Bulletin*, **100**, 1181–204.

Potyondy DO, Cundall PA, Lee CA (1996) Modeling rock using bonded assemblies of circular particles. In: *Rock Mechanics: Tools and Techniques* (eds Aubertin M, Hassani F, Mitri H), pp. 1937–44. Balkema, Rotterdam.

Pruess K (1991) TOUGH2—a general-purpose numerical simulator for multiphase fluid and heat flow, *Lawrence Berkeley Laboratory Report LBL-29400*, Lawrence Berkeley Laboratory, Berkeley, CA.

Renshaw CE, Harvey CF (1994) Propagation velocity of a natural hydraulic fracture in a poroelastic medium. *Journal of Geophysical Research*, **99**, 21667–77.

Saltzer SD, Pollard DD (1992) Distinct element modeling of structures formed in sedimentary overburden by extensional reactivation of basement normal faults. *Tectonics*, **11**, 165–74.

Schmitt GT (1954) Genesis and depositional history of Spraberry Formation, Midland Basin, Texas. *American Association of Petroleum Geologists Bulletin*, **38**, 1957–78.

Schmoker JW, Halley RB (1982) Carbonate porosity versus depth: a predictable relation for South Florida. *American Association of Petroleum Geologists Bulletin*, **66**, 2561–70.

Scholle PA (1980) A field guide to the geology of the Permian bank-to-basin section of the Guadalupe Mountains area, west Texas, and New Mexico. In: *Upper Paleozoic Depositional and Diagenetic Facies in a Mature Petroleum Province* (eds Scholle P, Halley R), pp. 1–139. U. S. Geological Survey Open-File Report 80-383. U. S. Geological Survey, Washington, DC.

Sclater JC, Christie PAF (1980) Continental stretching: an explanation of the post-mid-cretaceous subsidence of the central North Sea Basin. *Journal of Geophysical Research*, **85**, 3711–39.

Secor DT (1965) Role of fluid pressure in jointing. *American Journal of Science*, **263**, 633–46.

Stanley TB, Levinson SA, Masson PH, Pratt WL, Osanik A (1951) *Geological Investigation of the 'Spraberry'.* Unpublished report. Humble Oil and Refining Company, Midland Basin, West Texas.

Sterling JL (2000) *Fracture Generation and Fluids in the Spraberry Formation, Midland Basin, Texas.* Master's Thesis. New Mexico Institute of Mining and Technology, Socorro, New Mexico.

Sweeney JJ (1990) BASINMAT, FORTRAN program calculates oil and gas generation using a distribution of discrete activation energies. *Geobyte*, **37**, 37–43.

Tuncay K, Park A, Ortoleva P (2000) Sedimentary basin deformation: an incremental stress approach. *Tectonophysics*, **323**, 77–104.

Twiss RJ, Moores EM (1992) *Structural Geology*. W. H. Freeman and Company, New York.
Warn GF, Sidwell R (1953) Petrology of the Spraberry sands of West Texas. *Journal of Sedimentology and Petrology*, **23**, 67–74.
Winfree KE (1995) Post-Permian folding and fracturing of the Spraberry Formation within the Midland Basin region of west Texas. *West Texas Geological Society Bulletin*, **35**, 5–20.
Zoback ML, Zoback MD (1989) Tectonic stress field of the continental United States. *GSA Bulletin Memoir*, **172**, 523–39.

NOMENCLATURE

c empirical porosity coefficient associated with rock type
g acceleration of gravity$k$ intrinsic permeability
S_0 specific surface area
ϕ porosity
ϕ_0 estimated initial (surface) porosity
ρ_b bulk sediment density
ρ_w water density
σ total stress